RSC Advances

Molecular insights into the self-assembly of short amphiphilic peptides FmDn and FmKn

Journal:	*RSC Advances*
Manuscript ID:	RA-ART-09-2014-010571.R1
Article Type:	Paper
Date Submitted by the Author:	03-Nov-2014

Complete List of Authors:	Thota, Naresh; National University of Singapore, Department of Chemical and Biomolecular Engineering Ma, Yijia; National University of Singapore, Department of Chemical and Biomolecular Engineering Jiang, Jianwen; National University of Singapore, Department of Chemical and Biomolecular Engineering

Molecular insights into the self-assembly of short amphiphilic peptides F_mD_n and F_mK_n

Naresh Thota, Yijia Ma and Jianwen Jiang*

Department of Chemical and Biomolecular Engineering, National University of Singapore, 117576, Singapore

ABSTRACT

The self-assembly of short amphiphilic peptides F_mD_n and F_mK_n is investigated by molecular dynamics simulation. The peptides are composed of hydrophobic phenylalanine (Phe, F), as well as hydrophilic aspartic acid (Asp, D) and lysine (Lys, K), and described by coarse-grained MARTINI force field. Within μs-scale simulation, FD and FK only form loose polymeric clusters. Upon increasing the length of Phe residues in F_mD and F_mK (m = 2 to 4), larger and more stable micelles are formed. F_mK and F_mD prefer to assemble into quasi-spherical and sheet-like micelles, respectively. For F_3K_n (n = 2 to 8) and F_6K_n (n = 4 to 12), the assembly capability reduces leading to smaller micelles when the length of Lys residues increases. For the formation of quasi-spherical micelles with distinct core/shell structure, the optimal ratio of hydrophobic/hydrophilic residues is found to be 3/4 for both F_3K_n and F_6K_n. This simulation study provides molecular insights into the assembly process and mechanism of short peptides, and it could facilitate the development of new peptides with desired morphologies.

Keywords: residue, morphology, micelle, transition, simulation

*E-mail address: chejj@nus.edu.sg

1. Introduction

Amphiphiles can spontaneously self-assemble into a wide range of morphologies such as micelles, fibers, vesicles and sheets.[1-4] They have been commonly used in cosmetics, nano-fabrication, drug delivery and other applications.[5,6] Among various amphiphiles, biocompatible and biodegradable peptides are of particular interest. Compared with other materials, peptides display a high level of biological and chemical diversity. The assembled peptide structures can be readily tuned by tailoring the sequence, length and other conditions.[7] Earlier studies on the self-assembly of amphiphilic peptides involved relatively long sequences (more than 20 amino acids). However, the applications of long peptides are limited due to their high cost.[8] In this context, shorter amphiphilic peptides provide more economical alternatives.

A number of experimental and simulation studies have been reported on the self-assembly of short peptides. Notably, Zhang and coworkers examined surfactant-like peptides such as A_6D, V_6D, V_6D_2 and L_6D_2, which assembled into nanotubes and nanovesicles with an average diameter of 30 to 50 nm.[9] For A_3K, A_6K and A_9K, Xu et al. revealed that the morphologies changed from nanosheets to nanofibers upon increasing hydrophobic residues.[10] With a greater number of hydrophilic residues in A_6K_n, V_6K_n and L_6K_n (n = 1 to 5), vesicles were found to shift into nanotubes by Meng et al.[11] In a series of D_xF_y peptides, Siddique et al. observed micellar formation at larger x (more hydrophilic) and polymeric aggregation at larger y (more hydrophobic).[12] Recently, Wang et al. investigated the assembly of I_3K, which formed well-ordered nanotubes and showed effective encapsulation and sustained release of model drugs.[13]

On the other hand, molecular simulation studies have been also conducted on the self-assembly of short peptides. Simulation can provide important microscopic insights into the underlying mechanism of self-assembly and facilitate the rational development of new peptides towards desired morphologies. By using coarse-grained models, Frederix et al. simulated about 400 dipeptide combinations to screen possible dipeptides that can assemble

into typical morphologies.[14] Guo et al. found that diphenylalanine could form ordered structures like nanovesicles and further turned into nanotubes by vesicle fusion,[15] but triphenylalanine assembled into nanospheres and fully packed nanorods without any voids.[16] Combining simulation and experimental techniques, Hauser et al. examined the assembly of tri- to hexa-peptides into coiled fibers.[17]

The above studies highlight the central importance of the type and length of hydrophobic and hydrophilic residues in the self-assembly of short peptides. It remains a challenge to quantitatively understand the mechanism of self-assembly and the dynamic process of morphology transition. However, such understanding is indispensable to tailor assembled morphology for specific application.

In this study, molecular dynamics (MD) simulations were performed to examine the self-assembly of a series of short peptides F_mK_n and F_mD_n. The peptides contain phenylalanine (Phe, F), which is rather hydrophobic with a hydropathy index of 2.8.[18] It has a larger steric volume compared with other hydrophobic amino acids (e.g. A, V, L and I). Additionally, two type of hydrophilic residues, lysine (Lys, K) and aspartic acid (Asp, D) are present in these peptides. Following this introduction, the simulation models and methods are described in Section 2. In Section 3, the simulation results of F_mK and F_mD (m = 1 to 4) are first presented to examine how the type of hydrophilic residues and the length of hydrophobic residues affect self-assembly. Then, the results of F_3K_n and F_6K_n (n = 2 to 12) are presented to investigate the effect of the length of hydrophilic residues. The dynamic process and microscopic structures are analyzed in terms of the number of clusters, size distribution, the radii of micelle, core and shell, and the density profiles of residues. Finally, the concluding remarks are summarized in Section 4.

2. Models and methods

Fig. 1(a-c) illustrates the atomistic models of the three types of residues Phe, Asp and Lys. Self-assembly usually occurs in a microsecond time scale or even longer.[19,20] It is thus

computationally expensive to conduct atomistic simulation for self-assembly process. As an alternative, coarse-grained (CG) simulation is adopted in this study. In CG modeling, the number of degrees of freedom is reduced by mapping a group of atoms or molecules into a virtual interaction site. Although the atomistic details are lost, the essential molecular features are maintained in CG mapping. Consequently, the simulation time scale can be prolonged. Here, F_mK_n and F_mD_n peptides are represented by the MARTINI force field, which has been demonstrated to perform well for various systems such as peptides[21,22] and carbohydrates.[23] The MARTINI CG modeling uses 4:1 and 2/3:1 mappings for linear and cyclic molecules, respectively. Four main types of interaction sites are categorized as charged (Q), polar (P), nonpolar (N) and apolar (C). Further, these four types are categorized into 18 subtypes based on hydrogen bonding capability and polarity level, having a broad range of bead types to represent amino acids. Fig. 1(d-f) shows the CG models of Phe, Asp and Lys.

Fig. S1 and S2 in the ESI illustrate the atomistic and corresponding CG representations for all the peptides examined in this study. Table 1 lists the simulation conditions, including the number of peptides, box size, peptide concentration, and simulation duration. Each simulation system contained a certain number of peptides solvated in water. All peptides were assumed to be in random-coil conformations. To neutralize, chlorine (Cl^-) ions and sodium (Na^+) ions were added for F_mK_n and F_mD_n, respectively. Water and ions were also represented by the MARTINI force field. The simulation box was 11 nm for F_mK, F_mD and F_3K_n, but increased to 15 nm for F_6K_n with relatively longer chains. The concentrations of all peptides were approximately the same, equal to 75 mg/mL. In our previous study, the self-assembly of a long peptide FA32 was found to be independent of box size.[24] The system was initially energy minimized using the steepest descent method with a maximum step size of 0.005 nm and a force tolerance of 10 kJ mol^{-1} nm^{-1}. Then, the peptide positions were restrained and subject to 2 ns MD simulation in NPT (isothermal and isobaric) ensemble to allow water and ions to relax. Finally, MD simulation in NPT ensemble was performed 2500 ns for F_mK, F_mD and F_3K_n, and 5000 ns for F_6K_n. The minimization and MD simulation were conducted using GROMACS package (version 4.5.3).[25] Temperature was kept at 310 K, i.e.

the human body temperature, and controlled by the Berendsen method[26] with a time constant of 1 ps. Pressure was maintained at 1 bar with a time constant of 6 ps and a compressibility of 3×10^{-4} bar^{-1}. The periodic boundary conditions were applied in all three dimensions. The non-bonded Lennard−Jones (LJ) and electrostatic interactions were calculated using a cutoff of 1.2 nm. Furthermore, the standard shift function in GROMACS was used to reduce undesired noise. Consequently, the LJ and electrostatic interactions were shifted to zero from 0.9 and 0.0 nm, respectively, to the cutoff distance (1.2 nm). A time step of 20 fs was used for integration and trajectory was saved at every 1 ns interval. For analysis, the last 1000 ns trajectories were statistically averaged. The snapshots were captured using visual molecular dynamics (VMD) package.[27]

3. Results and discussion

First, F_mD and F_mK peptides are examined on how hydrophilic residues Asp and Lys, as well as the length of hydrophobic residues, affect self-assembly. Then, F_3K_n and F_6K_n peptides with different lengths of hydrophilic Lys residues are studied. For both cases, the assembly process and microscopic structures are analyzed in terms of the number of clusters, size distribution, radii of micelle, core and shell, and density profiles.

3.1 F_mD and F_mK Peptides

Fig. 2 shows the final snapshots for F_mD and F_mK (m = 1, 2, 3 and 4) at 2500 ns. Monomers, dimers, and loose polymeric clusters are observed for FD and FK, whereas all other peptides generally assemble into a single large cluster. Among this series peptides, FD and FK possess the weakest ability in assembly. With short hydrophobic block, the hydrophobic interaction in FD and FK is not sufficiently strong to allow the peptide forming a large cluster. The simulation study by Frederix et al. also predicted that FD and FK are difficult to assemble as their aggregation propensity (1.2) is less than the minimum (2.0) needed for assembly.[14] F_2D, F_3D, F_4D as well as F_2K form sheet-like structures with hydrophobic Phe (yellow) pointing inside and hydrophilic Asp/Lys (red) on the surface. Nevertheless, F_3K and F_4K assemble into quasi-spherical micelles.

The different assembly capabilities of F_mK and F_mD are due to the natures of Asp and Lys residues. Fig. 3 illustrates the energy minimized structures of F_3K, F_4K, F_3D and F_4D. Lys has a positively charged $–NH_3^+$ group in its side chain. The hydrogen atoms in $–NH_3^+$ tend to form intra-molecular H-bonding with the O and N atoms in peptide bond ($\begin{matrix} O & H \\ \| & | \\ -C- & N- \end{matrix}$) by bending the side chain. Therefore, the polar O and N atoms are embedded inside the molecule. In contrast, the side chain of Asp is relatively shorter and cannot easily bend to form intra-molecular H-bonding. Instead, inter-molecular H-bonds are formed in F_3D and F_4D, leading to the parallel arrangement of peptide chains and sheet-like structures. Comparing F_mK and F_mD, F_mK have great potential to form spherical micelles.

To analyze the dynamic assembly process, Fig. 4 plots the number of clusters (N_C) as a function of simulation time for F_mD and F_mK (m = 2, 3 and 4). If any two hydrophobic beads of different peptide chains are within a cutoff distance of 0.7 nm, the two peptides are considered to be in the same cluster. Initially, N_C is equal to the number of peptides added in the system as all peptides exist as monomers. For all cases, N_C drops dramatically in the first 150 ns due to the rapid formation of small clusters. Then the small clusters merge into larger clusters and finally a stable structure. This three-step assembly process was also observed for FA32 in our previous study.[24] Eventually, N_C approaches 1 for F_3D, F_4D, F_3K and F_4K. However, N_C fluctuates frequently for F_2D and F_2K, even in the last 500 ns simulation as demonstrated in the insets. The fluctuations are due to the formation of small clusters, as shown in Fig. 2, which can merge into and separate from the large cluster. Fundamentally, this is because the steric volume of hydrophobic F_2 is not sufficient to block hydrophilic residues from penetrating into hydrophobic core. For F_3D, F_4D, F_3K and F_4K, however, the stability of assembled cluster is enhanced with increasing the length of hydrophobic residues and hence hydrophobic interaction.

3.2 F_3K_n and F_6K_n Peptides

It is also intriguing to elucidate how the length of hydrophilic residues affects self-assembly. Fig. 5 shows the final snapshots for F_3K_n (n = 2, 3, 4, 5, 6 and 8) at 2500 ns. F_3K_2 forms a sheet-like cluster with Lys on the surface. Quasi-spherical micelles with distinct core/shell are

formed for F_3K_3, F_3K_4 and F_3K_5, particularly F_3K_4. Hydrophobic Phe (yellow) constitutes the central core and hydrophilic Lys (red) resides in the shell. With further increasing the length of Lys (F_3K_6 and F_3K_8), micelles still exist but with a smaller size, in addition to the presence of monomers and polymeric aggregates. Thus, the assembly capability is reduced as the length of hydrophilic residues increases. This behavior was also observed in our recent simulation study for FA32 derivatives.[28] The reason is that the hydrophobic interaction becomes relatively weaker, thus less strong assembly.

The assembly process for F_3K_n is characterized by the number of clusters N_C versus time. As shown in Fig. 6, N_C drops dramatically for F_3K_n (n = 2, 3, 4, 5, 6 and 8) in the initial 150 ns due to the rapid formation of small clusters. The N_C at 2500 ns is approximately equal to 1, 2, 4, 6, 8 and 11, respectively. As observed in Fig. 5, there is only 1 large cluster formed for F_3K_2 and the cluster is relatively stable with marginal fluctuation in N_C. For F_3K_3 and F_3K_4, N_C displays greater fluctuations between 1 and 7. With further increasing the length of Lys in F_3K_5, F_3K_6 and F_3K_8, the fluctuations are even greater between 2 and 16 due to the presence of polymeric aggregates. Obviously, increasing the length of Lys leads to weaker assembly.

The micelles formed are composed of hydrophobic core and hydrophilic shell. The radii of micelle, core and shell are estimated by[29]

$$R_{\text{micelle}} = \sqrt{\frac{1}{N}\sum_{i=1}^{N}(\mathbf{r}_i - \mathbf{r}_{\text{com}})^2} \quad (1)$$

$$R_{\text{core}} = \sqrt{\frac{1}{N}\sum_{i=1}^{N}(\mathbf{r}_{\text{HPB},i} - \mathbf{r}_{\text{com}})^2} \quad (2)$$

where N is the number of peptides in the micelle, $\mathbf{r}_{\text{com}}$ is the center-of-mass (COM) of the micelle, $\mathbf{r}_i$ and $\mathbf{r}_{\text{HPB},i}$ are the positions of outermost bead and hydrophobic bead in each peptide chain. The radius or thickness of shell (R_{shell}) is estimated by

$$R_{\text{shell}} = R_{\text{micelle}} - R_{\text{core}} \quad (3)$$

Fig. S3 plots the radii of micelle, core and shell for F_3K_2, F_3K_4 and F_3K_6. With increasing the length of Lys, R_{micelle} and R_{core} decrease, whereas R_{shell} increases slightly. The trend is accord with the final snapshots in Fig. 5. As discussed above, the assembly capability is

reduced and smaller micelles are formed for peptides with longer Lys. Similar to Fig. 6, greater fluctuations are also seen here with increasing the length of Lys. Table 2 lists the averaged values of $R_{micelle}$, R_{core} and R_{shell}. For F_3K_n (n = 2, 3, 4, 5, 6 and 8), the $R_{micelle}$ are 3.05, 2.21, 1.92, 1.75, 1.46 and 1.27 nm and the R_{core} are 2.59, 1.64, 1.30, 1.11, 0.89 and 0.72 nm, respectively. When the length of Lys increases, the size of micelle reduces. Consequently, the number of peptides in the micelle drops.

The values of radii in Table 2 are the averages of all the micelles formed in a system. However, various micelles differ in size and fluctuations occur during simulation. Thus, a size distribution would give more insightful information about the different sizes of micelles. Fig. 7 shows the distributions of $R_{micelle}$ for F_3K_n (n = 2, 3, 4, 5, 6 and 8). A single peak exists in the distribution for F_3K_2, narrowly ranging from 2.9 to 3.5 nm. This implies the formation of a single large cluster as observed in Fig. 5. For F_3K_3 and F_3K_4, there are two peaks indicating the presence of two different clusters. The peak centered at 1.0 nm is attributed to small clusters, while the other peak between 2.2 ~ 2.8 nm is due to the large clusters. Upon comparison, the distributions for F_3K_5, F_3K_6 and F_3K_8 are broader (between 1 to 3 nm). This is because of the weaker assembly capability with increasing the length of Lys leads to a wide variety of clusters, including monomer, dimer and polymeric aggregates. The distributions are consistent with the observation in Fig. 5.

The density profiles of residues versus the distance from the COM of a micelle were calcualted. As shown in Fig. S4, the density profiles for F_3K_2, F_3K_4 and F_3K_6 are generally similar, i.e., hydrophobic Phe residues reside dominantly in the core. For F_3K_2, the profile of Phe approaches zero at 4.5 nm because Phe also exists at the surface of sheet-like micelle (see Fig. 5). However, F_3K_4 forms quasi-spehrical micelle with distinct core/shell structure. Specifically, Phe resides in the core (0 – 1.5 nm) and Lys is primarly in the shell (1 – 3 nm). With further increasing the length of Lys, Lys also resides in the core as seen for F_3K_6. This is because hydrophobic interaction is weaken, which leads to the formation of small micelle and the disruption of core/shell structure. Based on the density profiles here and the snapshot in Fig. 5, F_3K_4 possesses beter potential than other F_3K_n to form quasi-micelles with disticnt

core/shell structure. Therefore, the optimal ratio of hydrophobic/hydrophilic residues tends to be 3/4.

We also evaluated the intermolecular LJ and electrostatic interactions between peptides for three peptides (F_3K, F_4K, and F_3K_2). As shown in Table S1, the LJ interactions are dominant over the electrostatic counterpart at both free (individual peptides) and aggregated states. This is because the interactions in the systems are primarily short ranged. Upon changing from free to aggregated state, the LJ and electrostatic interactions decrease (more negative), thus promoting the formation of clusters. Similar trend was also observed by Yu and Schatz in the simulation study of peptide amphiphile.[3]

To further explore the effect of the length of Lys, F_6K_n (n = 4, 6, 8, 10 and 12) were examined. As shown by the final snapshots in Fig. 8, the number of clusters is 1, 2, 3, 4, and 4, respectively. F_6K_4 assembles into an elliptical micelle. With increasing the length of Lys, micelles with distinct core/shell are formed. For F_6K_6, there are two micelles with different sizes, while the micelle size is nearly uniform for each of F_6K_8, F_6K_{10} and F_6K_{12}. Similar to Fig. 5 for F_3K_n, the micelle size reduces when the length of Lys increases. Compared with F_3K_n, however, fewer monomers are present in F_6K_n. Apparently, F_6K_n have stronger hydrophobic interaction than F_3K_n and thus stronger capability in assembly.

The number of clusters N_C versus time is plotted in Fig. 9 for F_6K_n (n = 4, 6, 8, 10 and 12). N_C remains a relatively stable value after 500 ns for each case. This duration (500 ns) is longer than that for F_3K_n (150 ns in Fig. 6), due to the increased peptide chain length and box size. Compared with F_3K_n, however, F_6K_n are more preferential in assembly and N_C exhibits much smaller fluctuations. Once a cluster is formed, hydrophilic residues will not easily move out from the cluster, which however happens more frequently for F_3K_n. As also observed in Fig. 8, N_C at equilibrium increases from F_6K_4 to F_6K_{12}. This is similar to F_3K_n, a consequence of reduced assembly upon increasing the length of Lys.

Fig. S5 shows the radii of micelle, core and shell for F_6K_4, F_6K_8 and F_6K_{12}. The $R_{micelle}$ fluctuates between 4 and 3 nm with increasing the length of Lys. Nevertheless, the fluctuations are smaller compared with F_3K_n in Fig. S3. The averaged $R_{micelle}$, R_{core} and R_{shell}

are listed in Table 2. For F_6K_n (n = 4, 6, 8, 10, and 12), the $R_{micelle}$ are 4.08, 3.48, 3.27, 3.22 and 3.34 nm, and the R_{core} are 3.53, 2.67, 2.11, 1.85 and 1.76 nm, respectively. Similar to the trend for F_3K_n, the micelle size reduces when the length of Lys increases.

The distributions of $R_{micelle}$ for F_6K_n are shown in Fig. 10. Pronounced peaks for F_6K_4, F_6K_6 and F_6K_8 are observed beyond 2.6 nm, indicating no presence of monomers. For F_6K_6, the two peaks suggest two micelles with different sizes as seen in Fig. 8. A major peak is centered at 3.5 nm for F_6K_{10} and F_6K_{12}, due to the formation of micelles with approximately uniform size. Additionally, a minor peak is also observed at 1.5 nm for F_6K_{10} and F_6K_{12}. This is attributed to the presence of small clusters (e.g. monomers), as the assembly capability is reduced for F_6K_{10} and F_6K_{12}.

The density profiles for F_6K_4, F_6K_8 and F_6K_{12} are shown in Fig. S6. For F_6K_4, Phe is the dominant residue in whole range, which implies no existence of distinct core/shell structure. This is indeed observed in Fig. 8 that F_6K_4 forms an elliptical micelle. For F_6K_8 and F_6K_{12}, distinct core/shell structure is seen with Phe in the core (0 – 2 nm) and Lys in the shell (1 – 3.5 nm). Upon comparison between F_3K_n and F_6K_n, the latter forms larger and more stable structures due to longer Phe residues. Nevertheless, the optimal ratio of hydrophobic/hydrophilic residues seems to be 3/4 for both F_3K_n and F_6K_n to form quasi-spherical micelles.

4. CONCLUSION

We have simulated the self-assmbly of a series of short peptides F_mD_n and F_mK_n. F_mK_n have stronger capability to form quais-spherical micelles, while F_mD_n tend to form sheet-like structures. With increasing the length of hydrophilic Lys residues in both F_3K_n and F_6K_n, smaller and less stable micelles are formed with larger fluctuations; thus the assembly capability decreases. Compared with F_3K_n, nevertheless, F_6K_n possess more hydrophobic Phe residues and hence stronger assembly capability. It can be concluded that hydrophobic interaction plays a key role for peptides to assemble. Moreover, F_3K_4 and F_6K_8 are found to form quasi-spherical micelles with distinct core/shell structure (Phe in the core and Lys in the

shell). The optimal ratio of hydrophobic/hydrophilic residues appears to be 3/4. Upon increasing this ratio, quasi-spherical micelles tend to shift to elliptical aggregates; while decreasing this ratio leads to smaller and less stable micelles. This ratio found here is signifcant as it can assist in the rational selection of appropriate F_mK_n peptides to assemble into spherical micelles. It should be noted, however, this ratio may depend on the type of residue by varying steric volume and hydrophobicity, and thus may not be the same for other peptides. Overall, the simulation study reported here provides insightful information about the dynamic assembly and microsocpic morphology of F_mD_n and F_mK_n. With this knowledge, different nanostructures could be obtained towards potential applications.

Acknowledgements

The authors gratefully acknowledge the National University of Singapore and the Ministry of Education of Singapore (R-279-000-353-112) for financial support.

Electronic Supplementary Information

Atomistic and coarse-grained representations of peptides, radii of micelle, core and shell, density profiles, interaction energies at free and aggregated states.

References

1 W. A. Petka, J. L. Harden, K. P. McGrath, D. Wirtz and D. A. Tirrell, *Science*, 1998, **281**, 389.

2 Y. S. Velichko, S. I. Stupp and M. O. de la Cruz, *J. Phys. Chem. B*, 2008, **112**, 2326.

3 T. Yu and G. C. Schatz, *J. Phys. Chem. B*, 2013, **117**, 9004.

4 T. Yu, O.-S. Lee and G. C. Schatz, *J. Phys. Chem. A*, 2013, **117**, 7453.

5 M. Lazzari, C. Rodriguez-Abreu, J. Rivas and M. A. Lopez-Quintela, *J. Nanosci. Nanotechno.*, 2006, **6**, 892.

6 J. M. Mason, *Future Med. Chem.*, 2010, **2**, 1813.

7 X. B. Zhao, F. Pan, H. Xu, M. Yaseen, H. H. Shan, C. A. E. Hauser, S. G. Zhang and J. R. Lu, *Chem. Soc. Rev.*, 2010, **39**, 3480.

8 S. Koutsopoulos, L. Kaiser, H. M. Eriksson and S. Zhang, *Chem. Soc. Rev.*, 2012, **41**, 1721.

9 S. Vauthey, S. Santoso, H. Gong, N. Watson and S. Zhang, *Proc. Natl. Acad. Sci. (USA)*, 2002, **99**, 5355.

10 H. Xu, J. Wang, S. Han, J. Wang, D. Yu, H. Zhang, D. Xia, X. Zhao, T. A. Waigh and J. R. Lu, *Langmuir*, 2008, **25**, 4115.

11 Q. Meng, Y. Kou, X. Ma, Y. Liang, L. Guo, C. Ni and K. Liu, *Langmuir*, 2012, **28**, 5017.

12 B. Siddique and J. Duhamel, *Langmuir*, 2011, **27**, 6639.

13 Q. Wang, X. Zhang, J. Zheng and D. Liu, *RSC Adv.*, 2014, **4**, 25461.

14 P. W. J. M. Frederix, R. V. Ulijn, N. T. Hunt and T. Tuttle, *J. Phys. Chem. Lett.*, 2011, **2**, 2380.

15 C. Guo, Y. Luo, R. Zhou and G. Wei, *ACS Nano*, 2012, **6**, 3907.

16 C. Guo, Y. Luo, R. Zhou and G. Wei, *Nanoscale*, 2014, **6**, 2800.

17 C. A. E. Hauser, R. Deng, A. Mishra, Y. Loo, U. Khoe, F. Zhuang, D. W. Cheong, A. Accardo, M. B. Sullivan, C. Rieker, J. Y. Ying and U. A. Hauser, *Proc. Natl. Acad. Sci. (USA)*, 2011, **108**, 1361.

18 D. L. Nelson, A. L. Lehninger and M. M. Cox, *Lehninger Principles of Biochemistry*. W.H. Freeman, New York, **2008**.

19 M. L. Klein and W. Shinoda, *Science*, 2008, **321**, 798.

20 M. McCullagh, T. Prytkova, S. Tonzani, N. D. Winter and G. C. Schatz, *J. Phys. Chem. B*, 2008, **112**, 10388.

21 O.-S. Lee, V. Cho and G. C. Schatz, *Nano Lett.*, 2012, **12**, 4907.

22 T. Yu and G. C. Schatz, *J. Phys. Chem. B*, 2013, **117**, 14059.

23 C. A. López, A. J. Rzepiela, A. H. de Vries, L. Dijkhuizen, P. H. Hünenberger and S. J. Marrink, *J. Chem. Theory Comput.*, 2009, **5**, 3195.

24 N. Thota, Z. Luo, Z. Hu and J. Jiang, *J. Phys. Chem. B*, 2013, **117**, 9690.

25 B. Hess, C. Kutzner, D. van der Spoel and E. Lindahl, *J. Chem. Theory Comput.*, 2008, **4**, 435.

26 H. J. C. Berendsen, J. P. M. Postma, W. F. van Gunsteren, A. DiNola and J. R. Haak, *J. Chem. Phys.*, 1984, **81**, 3684.

27 W. Humphrey, A. Dalke and K. Schulten, *J. Mol. Graphics*, 1996, **14**, 33.

28 N. Thota and J. Jiang, *J. Phys. Chem. B*, 2014, **118**, 2683.

29 Z. Luo and J. Jiang, *J. Controlled Release*, 2012, **162**, 185.

Table 1. Simulation conditions.

Peptide	Number of peptides	Box size (nm)	Peptide concentration (mg/mL)	Simulation duration (ns)
FD	171	11	74.87	2500
FK	142	11	74.93	2500
F_2D	108	11	75.17	2500
F_2K	95	11	74.66	2500
F_3D	79	11	75.38	2500
F_3K	72	11	75.17	2500
F_4D	62	11	75.17	2500
F_4K	58	11	75.53	2500
F_3K_2	58	11	76.18	2500
F_3K_3	48	11	75.98	2500
F_3K_4	41	11	75.94	2500
F_3K_5	36	11	76.39	2500
F_3K_6	31	11	74.13	2500
F_3K_8	26	11	76.18	2500
F_6K_4	72	15	74.59	5000
F_6K_6	60	15	74.91	5000
F_6K_8	51	15	74.51	5000
F_6K_{10}	45	15	75.31	5000
F_6K_{12}	40	15	75.44	5000

Table 2. Number of micelles, peptides per micelle, radii of micelle, core and shell.

peptide	number of micelles	peptides per micelle	$R_{micelle}$ (nm)	R_{core} (nm)	R_{shell} (nm)
F_3K_2	1	57 ± 1	3.05 ± 0.15	2.59 ± 0.16	0.46 ± 0.04
F_3K_3	2	24 ± 4	2.21 ± 0.38	1.64 ± 0.30	0.57 ± 0.11
F_3K_4	4	13 ± 3	1.92 ± 0.34	1.30 ± 0.24	0.63 ± 0.12
F_3K_5	6	8 ± 2	1.75 ± 0.32	1.11 ± 0.20	0.64 ± 0.14
F_3K_6	8	6 ± 4	1.46 ± 0.30	0.89 ± 0.18	0.57 ± 0.14
F_3K_8	11	2 ± 1	1.27 ± 0.26	0.72 ± 0.16	0.55 ± 0.13
F_6K_4	1	72	4.08 ± 0.06	3.53 ± 0.07	0.56 ± 0.04
F_6K_6	2	30 ± 12	3.48 ± 0.15	2.67 ± 0.16	0.81 ± 0.05
F_6K_8	3	17 ± 3	3.27 ± 0.05	2.11 ± 0.04	1.16 ± 0.06
F_6K_{10}	4	11 ± 3	3.22 ± 0.14	1.85 ± 0.07	1.37 ± 0.09
F_6K_{12}	4	10 ± 2	3.34 ± 0.26	1.76 ± 0.13	1.58 ± 0.16

Fig. 1 Atomistic and coarse-grained models of Phe (a, d), Asp (b, e) and Lys (c, f), respectively. Color codes for (a), (b) and (c): N, blue; O, red; C, cyan and H, white.

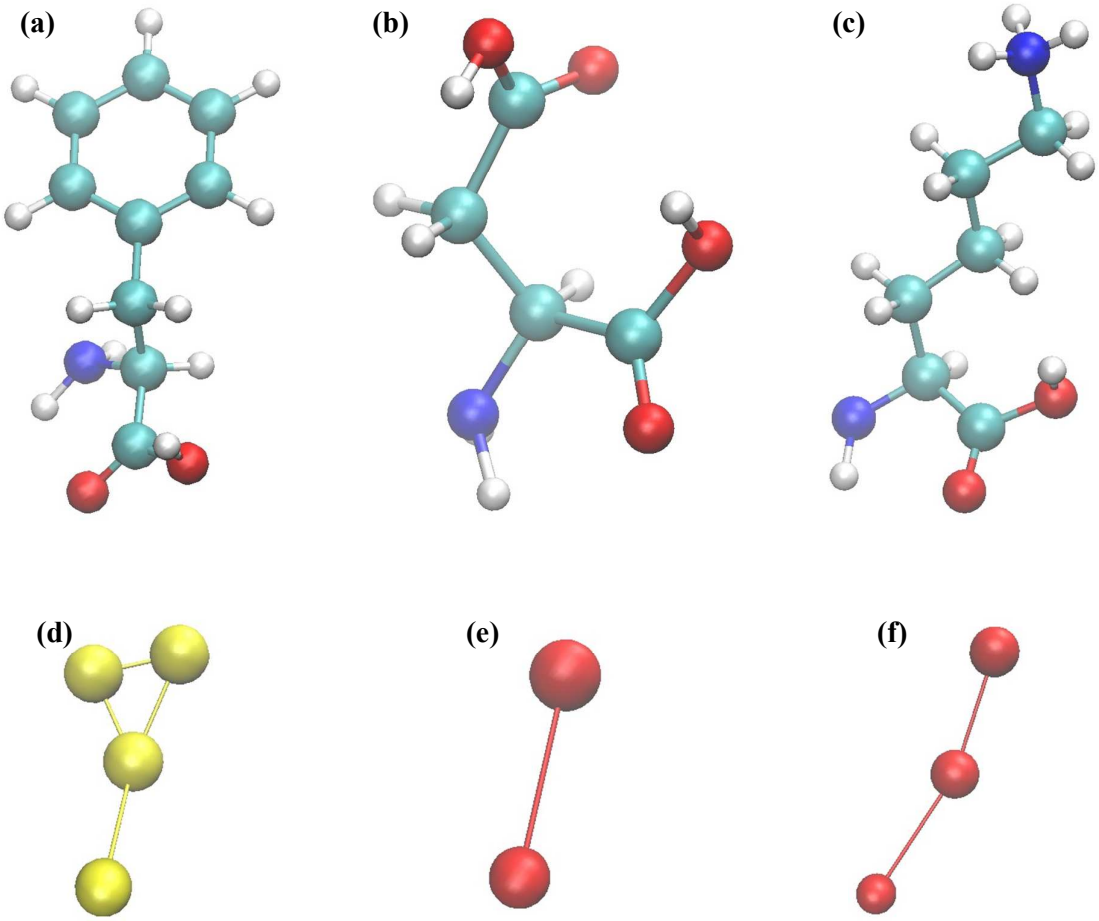

Fig. 2 Final snapshots for F_mD and F_mK (m = 1, 2, 3 and 4) at 2500 ns. Phe: yellow, Asp and Lys: red. Water and ions are not shown for clarity.

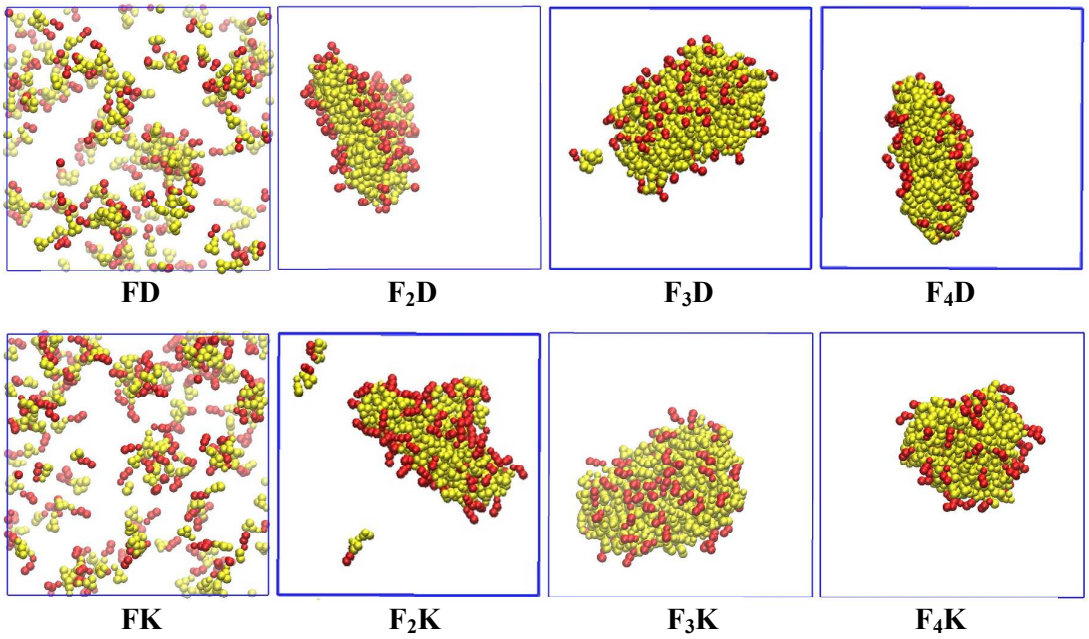

Fig. 3 Energy minimized structures of F_3K, F_4K, F_3D and F_4D.

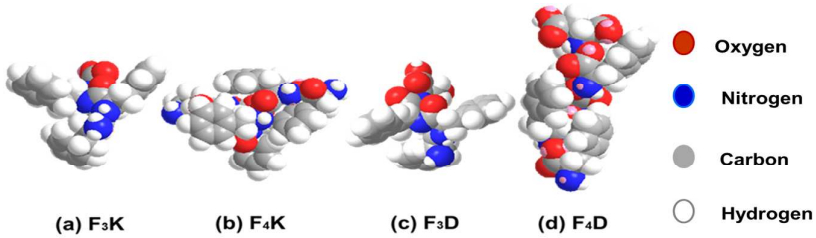

Fig. 4 Number of clusters versus time for F_mD and F_mK (m = 2, 3 and 4).

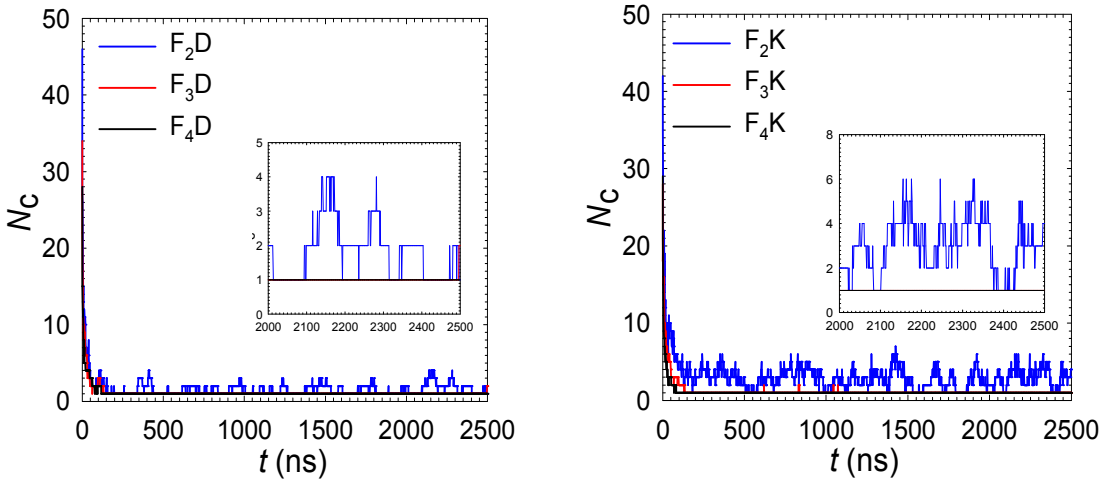

Fig. 5 Final snapshots for F_3K_n (n = 2, 3, 4, 5, 6 and 8) at 2500 ns. Phe: yellow, Lys: red. Water and ions are not shown for clarity.

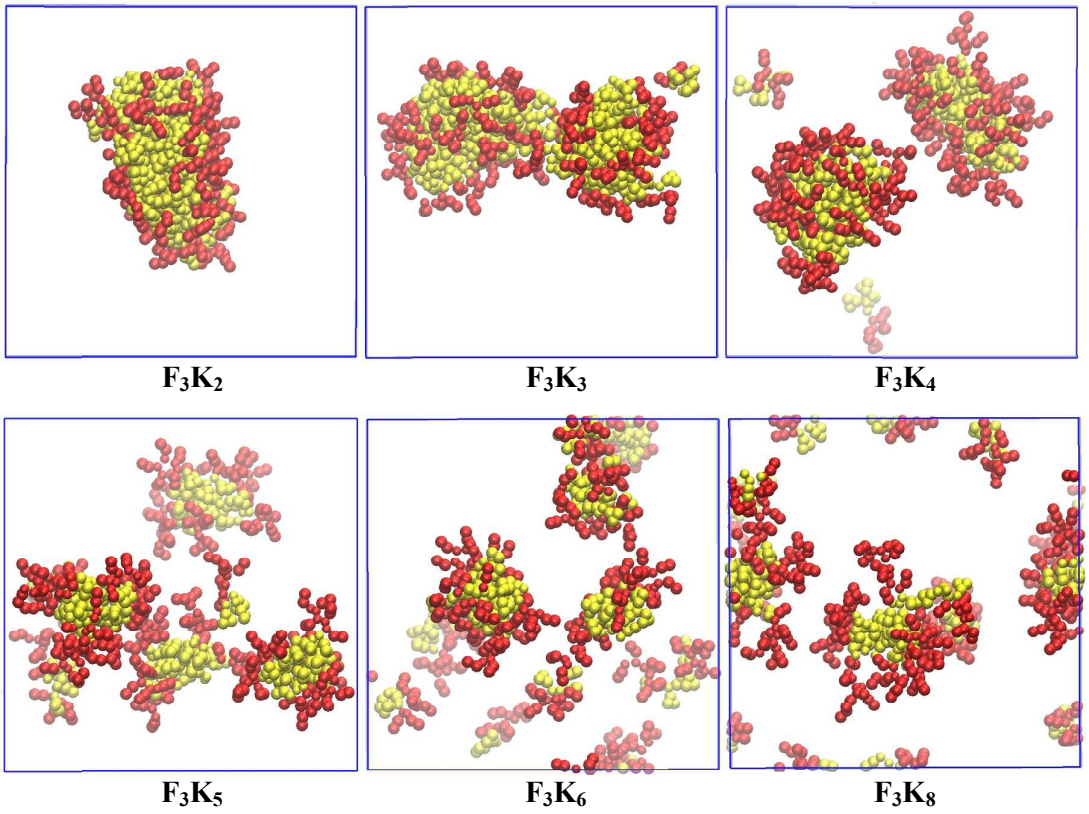

Fig. 6 Number of clusters versus time for F_3K_n (n = 2, 3, 4, 5, 6 and 8).

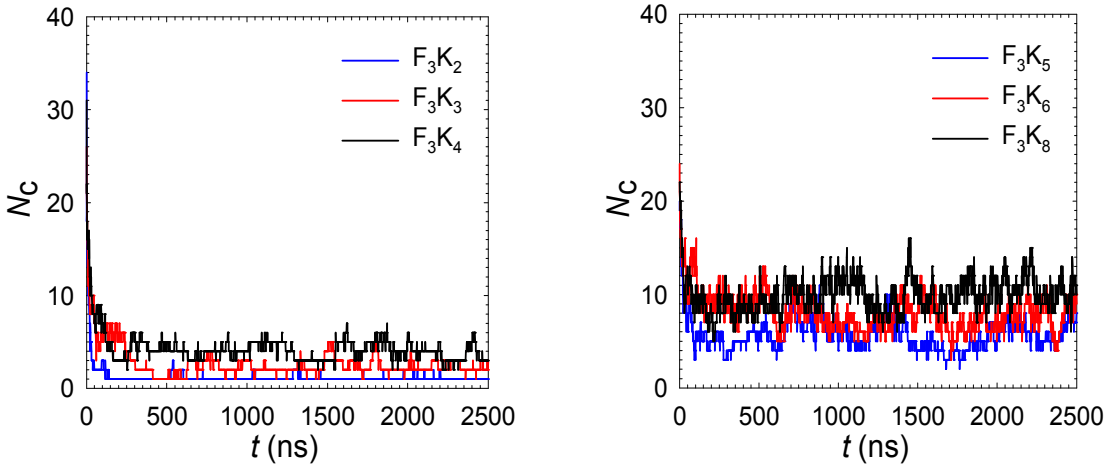

Fig. 7 Distributions of $R_{micelle}$ for F_3K_n (n = 2, 3, 4, 5, 6 and 8).

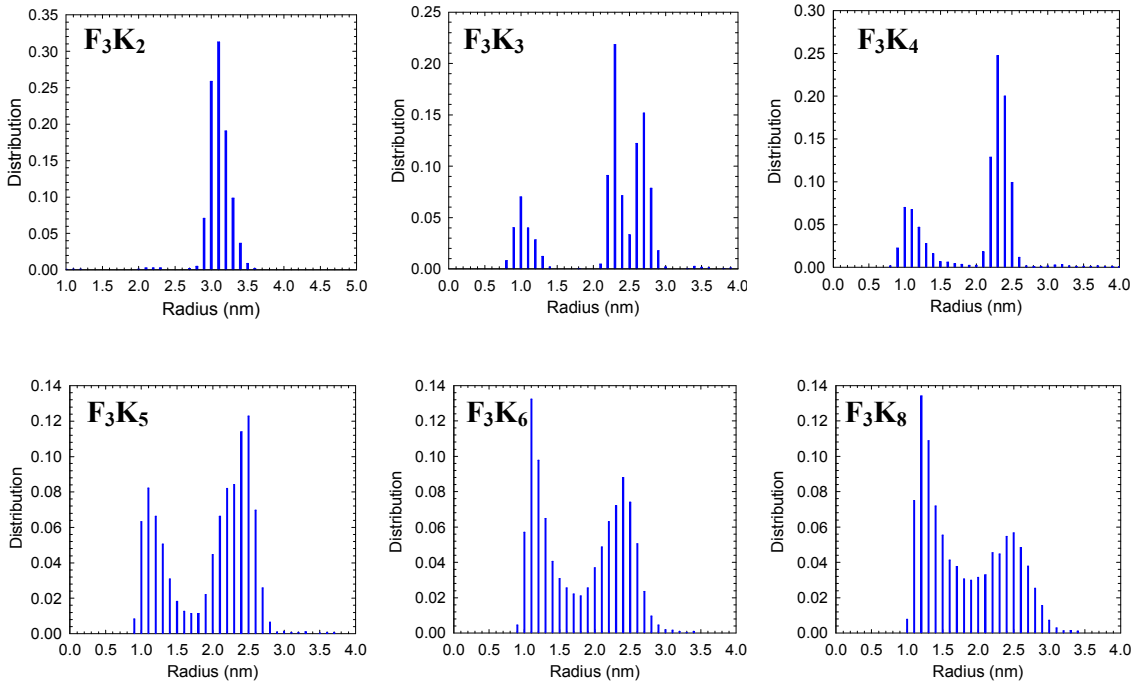

Fig. 8 Final snapshots for F_6K_n (n = 4, 6, 8, 10 and 12) at 5000 ns. Phe: yellow, Lys: red. Water and ions are not shown for clarity.

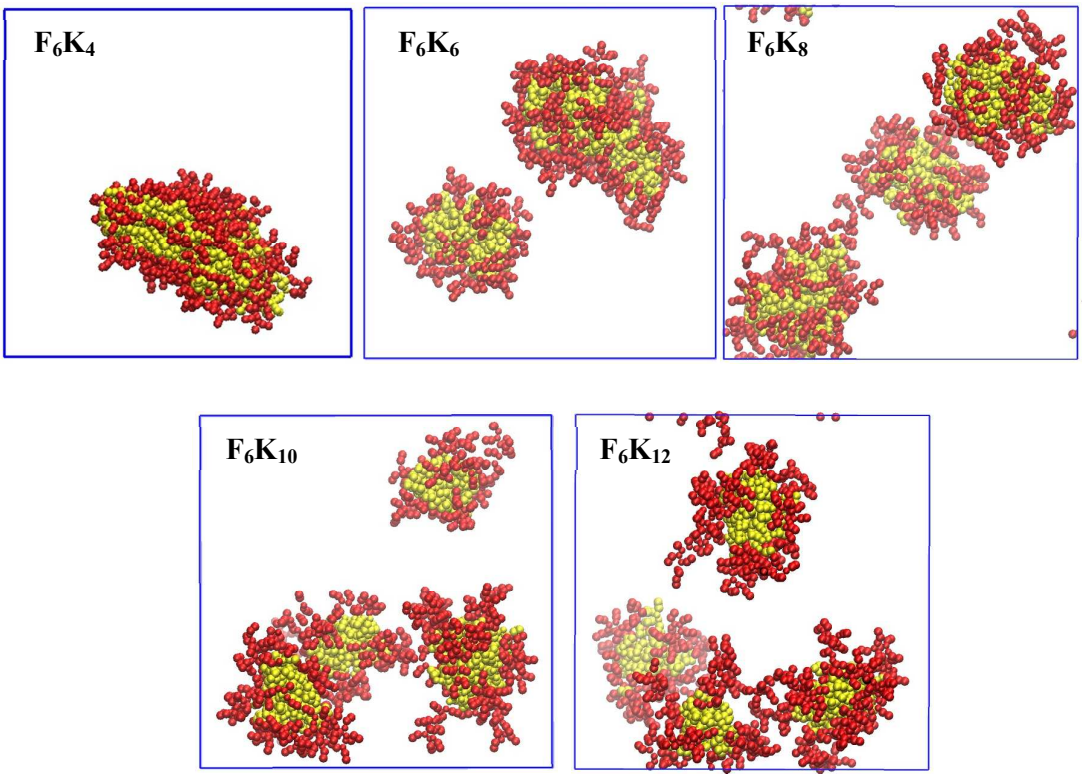

Fig. 9 Number of clusters versus time for F_6K_n (n = 4, 6, 8, 10 and 12).

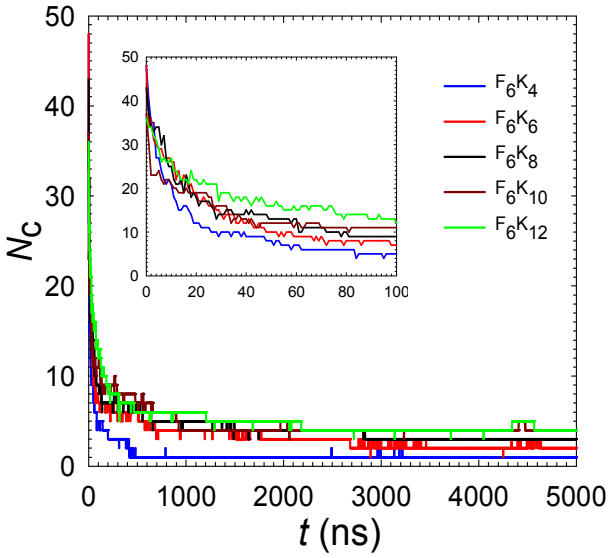

Fig. 10 Distributions of $R_{micelle}$ for F_6K_n (n = 4, 6, 8, 10 and 12).

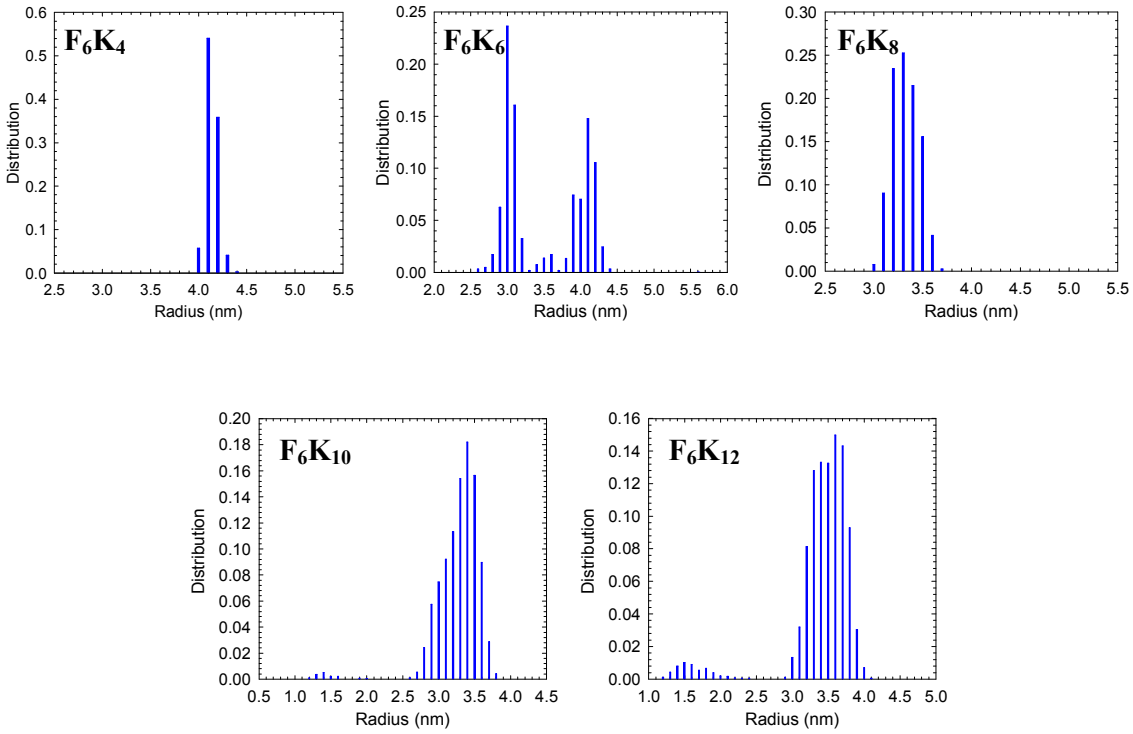

Table of Contents Graphic

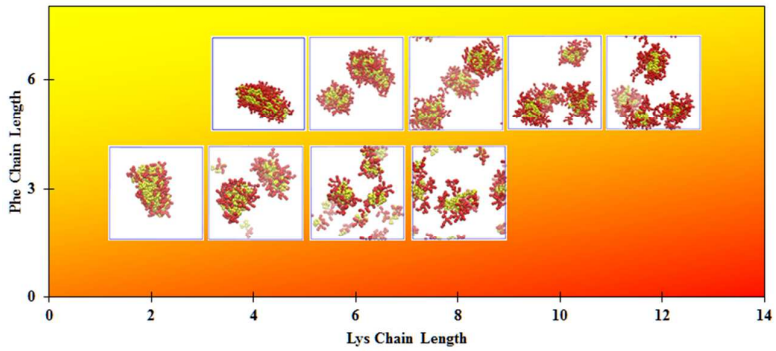

Molecular dynamics simulation is reported for the self-assembly of short amphiphilic peptides F_mD_n and F_mK_n.